PLANT SCIENCES

On-site identification of ozone damage in fruiting plants using vapor-deposited conducting polymer tattoos

Jae Joon Kim[1]*, Ruolan Fan[1]*, Linden K. Allison[1], Trisha L. Andrew[1,2†]

Climate change is leading to increased concentrations of ground-level ozone in farms and orchards. Persistent ozone exposure causes irreversible oxidative damage to plants and reduces crop yield, threatening food supply chains. Here, we show that vapor-deposited conducting polymer tattoos on plant leaves can be used to perform on-site impedance analysis, which accurately reveals ozone damage, even at low exposure levels. Oxidative damage produces a unique change in the high-frequency (>10^4 Hz) impedance and phase signals of leaves, which is not replicated by other abiotic stressors, such as drought. The polymer tattoos are resilient against ozone-induced chemical degradation and persist on the leaves of fruiting plants, thus allowing for frequent and long-term monitoring of cellular ozone damage in economically important crops, such as grapes and apples.

INTRODUCTION

Common air pollutants and excess nitrates in topsoil react with environmental oxygen in the presence of ultraviolet (UV) radiation to produce nontrivial amounts of ground-level ozone (*1*). In turn, prolonged exposure to ground-level ozone causes irreversible oxidative damage to living plants and decreases the yield of many important food crops (*1*, *2*). Ozone damage is predicted to become an increasing threat to global food production due to climate change (*3*, *4*). At present, late-stage visual identification (*5*, *6*) of necrotized leaf tissue, followed by off-site laboratory confirmation of reactive oxygen species in digested samples, is the predominant method of recording ozone damage in crops (*7*, *8*). However, visual observation cannot reveal early-stage ozone damage, and many commonplace abiotic stressors, such as drought, could also result in necrotized leaf tissue, preventing on-time interventions (*7*, *9*). Biochemical assays require time and dedicated facilities and cannot be easily performed on-site or on demand, meaning that temporal information is lost during the process of sampling, digesting, and assaying field samples. External ozone gas detectors that are inserted into the soil do not reveal tissue damage (*10*), and stomatal flow detectors that are adhered to plant surfaces (*11*, *12*) only yield useable data after months or years of continuous monitoring (*13*, *14*).

Burgeoning efforts in the area of plant electronics have established the benefits of integrating nanomaterials and/or microelectronics with living plants. Advances include the ability to enhance native light absorption for improved photosynthesis (*15*) and transpiration (*16*), to evolve unprecedented functionalities such as bioluminescence (*17*, *18*) and energy generation (*19*, *20*), and to create internal electrical connections (*21*, *22*) and device components (*23*, *24*) within the plant. Unique plant-based sensor systems have also been developed by either implanting (*23*, *25*) or decorating the surfaces of plants with conductive electrodes (*26*) to measure electrical signals arising from hydration (*27*), plant growth, and environmental humidity (*28*, *29*). However, the particular problem of detecting early-stage ozone damage has not yet found a viable solution. Furthermore, many existing nanomaterials cannot be invoked because of their poor chemical stability upon exposure to reactive oxygen species. To solve these problems, ozone tolerant materials and reliable, on-site measurement techniques for revealing biological ozone damage are necessary.

RESULTS

We selected grapes (*Vitis vinifera* L.) as our model plant because the fruit yield (*30*) and fruit quality (*31*, *32*) of grapevines decrease substantially upon exposure to ground level ozone, resulting in notable economic losses. As illustrated in Fig. 1, the primary points of entry for ozone are the stomata located on the underside (abaxial face) of leaves. Oxidative damage and necrotization begins around these abaxial faces, through the stomata, and slowly spreads across the rest of the leaf and plant. However, oxidative damage is difficult to visually observe from either the front or back face of the leaf, particularly at low ozone exposure levels. The limitations of optical detection (*9*) are evident in Fig. 1 and fig. S1—nonuniform and slow cell death over small areas do not lead to a clear visual change, especially when using drone photography performed under varying sunlight intensities and atmospheric haze. Leaf necrotization is clear only at high ozone doses, approximately >15 ppmh, at which point systemic shutdown would have already commenced [an ozone dose of 20 ppmh has been established to result in a permanent 10% decrease in grape production across different grape varieties (*30*)]. Prior work established the efficacy of using impedance spectroscopy to study ozone damage in native trees (*33*). We set out, therefore, to build on this work and create a long-lasting electrode interface so that impedance measurements can be performed on-site and on demand over many growth seasons.

A selected set of electrode materials and formulations were investigated, ranging from colloidal inks, an aqueous conducting polymer formulation [poly(3,4-ethylenedioxythiophene)-poly(styrene sulfonate) (PEDOT:PSS)] and a vapor-deposited conducting polymer tattoo, PEDOT-Cl, created using oxidative chemical vapor deposition (oCVD) following our previously reported procedure (*26*). After

[1]Department of Chemistry, University of Massachusetts Amherst, Amherst, MA 01003, USA. [2]Department of Chemical Engineering, University of Massachusetts Amherst, Amherst, MA 01003, USA.
*These authors contributed equally to this work.
†Corresponding author. Email: tandrew@umass.edu

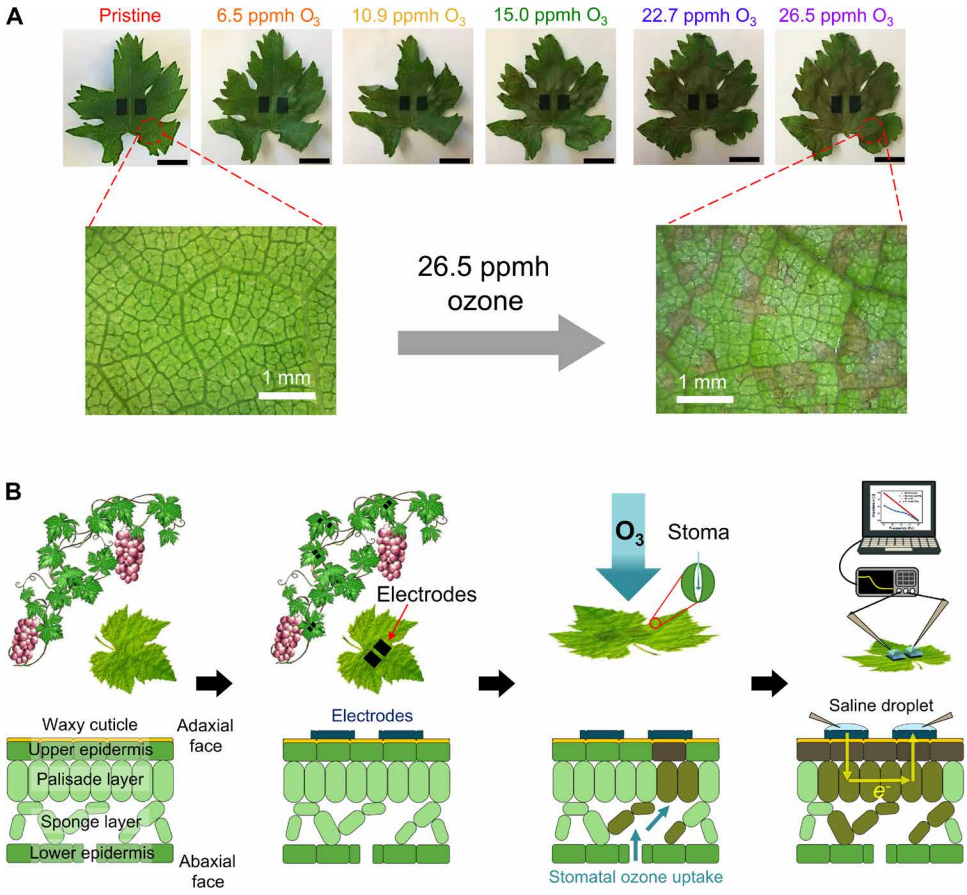

Fig. 1. Oxidative damage of leaf tissue by ozone exposure. (**A**) Pictures of a grape leaf exposed to various doses of ozone. Scale bars, 10 mm. Optical microscope images (10×) of a pristine grape leaf and the same leaf after exposure to a 26.5 ppmh dose of ozone are provided in the second row. Photo credit: Jae Joon Kim, University of Massachusetts Amherst. (**B**) Scheme of impedance-based detection of ozone damage in fruiting plants.

depositing on grape leaves, their properties were studied and summarized in Table 1 and fig. S2. Colloidal metal and conductive carbon inks have previously been used to decorate flowers with circuit patterns using creative screen and transfer printing techniques (*34*). In this case, however, we found grape leaves to be a challenging surface to coat. The hairy, hydrophobic surface of the grape leaf (fig. S3) restricted the shape of PEDOT:PSS electrodes to patterns created by uncontrollable droplets, and the resulting PEDOT:PSS electrodes could be easily washed away with water (fig. S2). In the case of silver and graphite, it was necessary to concentrate the commercial pastes and increase their viscosity such that a persistent electrode film was left behind on the leaf upon drying. These fabrication limitations resulted in rough, micrometer-thick electrodes that were easily cracked and/or delaminated from the leaf surface upon bending and exposure to environmental humidity (fig. S2). Moreover, the solvent used to create silver and graphite electrodes was found to visibly decolor and degrade the underlying leaf. Vapor-deposited PEDOT-Cl tattoos did not suffer from any of these disadvantages. PEDOT-Cl tattoos could be easily patterned to various angular shapes with clear boundary lines and demonstrated strong adhesion to the underlying hydrophobic leaf surface, without cracking or delamination. As reported previously (*26*), the process of oCVD did not chemically or physically damage the grape leaves used here, and cut stems with tattooed leaves could be placed in water with a rooting hormone to stimulate root growth. The long-term stability of vapor-deposited tattoos on live seedlings was also explored in our previous study (*26*), and neither microcracks nor eroded/faded areas were observed in the polymer tattoos after 18 months, over which time the tattooed seedlings grew new roots and leaves and matured into a healthy, still-thriving adult plant.

Electrode conductivities were also compared before and after exposure to 26.5 ppmh ozone. Ozone oxidizes metal thin films to their respective oxides (*35*) and creates epoxide and carboxylic acid defects in carbon allotropes (*36*), which compromises the conductivity and long-term stability of these electrode materials. When tested on glass substrates, very thick silver electrodes (>5 μm) were needed to mitigate ozone-induced destruction of electrical conductivity; thinner films suffered from up to a 30% reduction in surface conductivity with ozone exposure. The conductivity of the graphite electrodes initially increased with ozone treatment, likely due to the formation of mobile ionic species, but decreased gradually over time as these mobile ions were washed out of the electrodes during subsequent measurements. The conductivity of PEDOT:PSS immediately and severely decreased to 33% of its original value after ozone exposure. Based on previous reports, we hypothesized that the PSS component solubilized and retained reactive oxygen species within the film, which caused accelerating chemical damage over time and negatively affected the electrical stability of PEDOT:PSS

Table 1. Comparison of different electrode coatings on grape leaves.

Electrode properties	PEDOT-Cl	PEDOT:PSS	Silver	Graphite
Deposition solvent	–	Water (pH 2)	Acetone	Isopropyl alcohol
Thickness	1 μm	3–5 μm	3–5 μm	3–5 μm
Flex stability (Δσ after applying 10% strain)	5%	∞ (cracked)	∞ (cracked)	∞ (cracked)
Surface adhesion to rinsing (rinse with tap water flow)	Strong	Dissolved	Peels off	Peels off
Solution stability (σ change, water/saline)	106, 134%	0, 0% (dissolved)	100, 100%	95, 106%
Ozone stability* (26.5 ppmh dose)	105%	33%	98%	146%
Tissue damage (visual inspection)	None	None	Severe	Little
Patterning resolution	μm	cm	mm	mm
Transmittance* (450, 677 nm)	48, 16%	76, 56%	0, 0%	0, 0%

*Measured using films deposited on glass.

(*37*). In contrast, PEDOT-Cl films (400-nm-thick and 1-μm-thick films) created using oCVD did not display a notable decrease in conductivity upon exposure to the same dose of ozone, most likely because of poor ozone penetration into the comparatively crystalline films (*38*, *39*).

For long-term applications, any electrode placed on the surface of a leaf needs to exhibit high transmittance of visible light so that underlying chloroplasts can absorb sufficient photons for photosynthesis. From the results in Fig. 2A, PEDOT:PSS and PEDOT-Cl electrodes exhibited high transmittance at 450 nm (76 and 48%, respectively), while the silver and graphite electrodes reflected and/or absorbed most of the light in this region. Moreover, the transmittance of PEDOT-Cl at 450 nm could be increased to 70% by depositing thinner polymer layers (Fig. 2D).

Nondestructive impedance measurements were performed by placing a saline droplet directly on each electrode coating (fig. S4) and inserting probe tips into the saline droplet. The saline layer eliminated the problem of varying contact area and contact resistance between the rigid metallic probe tip (that is connected to the impedance analyzer) and the various flexible electrode coatings studied here. The ionic strength and viscosity of this saline layer did not affect the resulting impedance signal; therefore, for real-world applications, a variety of commercial saline gel formulations can be used to perform on-site impedance measurements. As shown in fig. S5, the conduction pathway is composed of the electrode/leaf contact area and various cellular structures defined by membranes. The biological state of the leaf will be revealed by collectively interpreting the impedance and phase signals obtained as a function bias frequency. Each frequency range reveals information about the strength and status of different tissue components (*40*, *41*), and therefore, it is important for an ideal electrode material to provide accurate impedance and phase signals over a broad frequency range. However, in the case of PEDOT:PSS, no clear signal could be observed from a grape leaf in the high-frequency (10^3 to 10^6 Hz) range (Fig. 2E), called the beta dispersion region (*42*, *43*), because of nonideal electrode contact to the underlying leaf tissue (the observed impedance signal could be assigned entirely to the PEDOT:PSS electrode itself). In the case of graphite and silver electrodes, impractically high impedance values were observed due to the large electrical mismatch between the metallic electrode material and leaf tissue. Most detrimentally, an especially high resistance and a large phase mismatch were observed in the alpha dispersion region (<10^3 Hz) (*43*) because of poor electronic charge transfer efficiency (Fig. 2F). On the other hand, PEDOT-Cl electrodes afforded signals arising from cellular components in a grape leaf in both the alpha and beta dispersion regions, without suffering from large phase or impedance mismatches. This observation confirmed that the interaction between vapor-deposited PEDOT-Cl electrodes and the plant epidermis was strong enough to enable a sensitive and efficient electronic interface.

In total, we concluded that vapor-deposited PEDOT-Cl tattoos were the most practical electrode candidates for on-site ozone detection because of their nondestructive nature, mechanical and long-term electronic stability (particularly against ozone degradation), tunable transparency, and ability to provide a controllable and reliable electrical interface to leaf tissue (fig. S6).

PEDOT-Cl tattoos were created on freshly cut grape leaves, and these samples were then exposed to controlled and continuous ozone doses using an ozone generator. The calibration curve for quantifying the generated ozone dose across various exposure times is provided in fig. S7. The impedance- and phase-frequency plots obtained for grape leaves exposed to various ozone doses are shown in Fig. 3 (representative curves for measurements performed on 20 different grape leaves are plotted). The impedance in the high-frequency region (10^4 to 10^6 Hz) linearly increased with ozone exposure until it saturated at high ozone doses (>22.7 ppmh). Ozone-induced changes were more obvious in the phase-frequency plot, where the peak phase at 10^5 Hz shifted from −42° to −16°. The estimated limit of detection, defined as the ozone dose at which a three times decrease in the phase signal could be observed relative to the variance (noise) of the measurement performed across multiple healthy grape leaves, was approximately 10 ppmh, which is lower than the estimated dose at which fruit yields suffer.

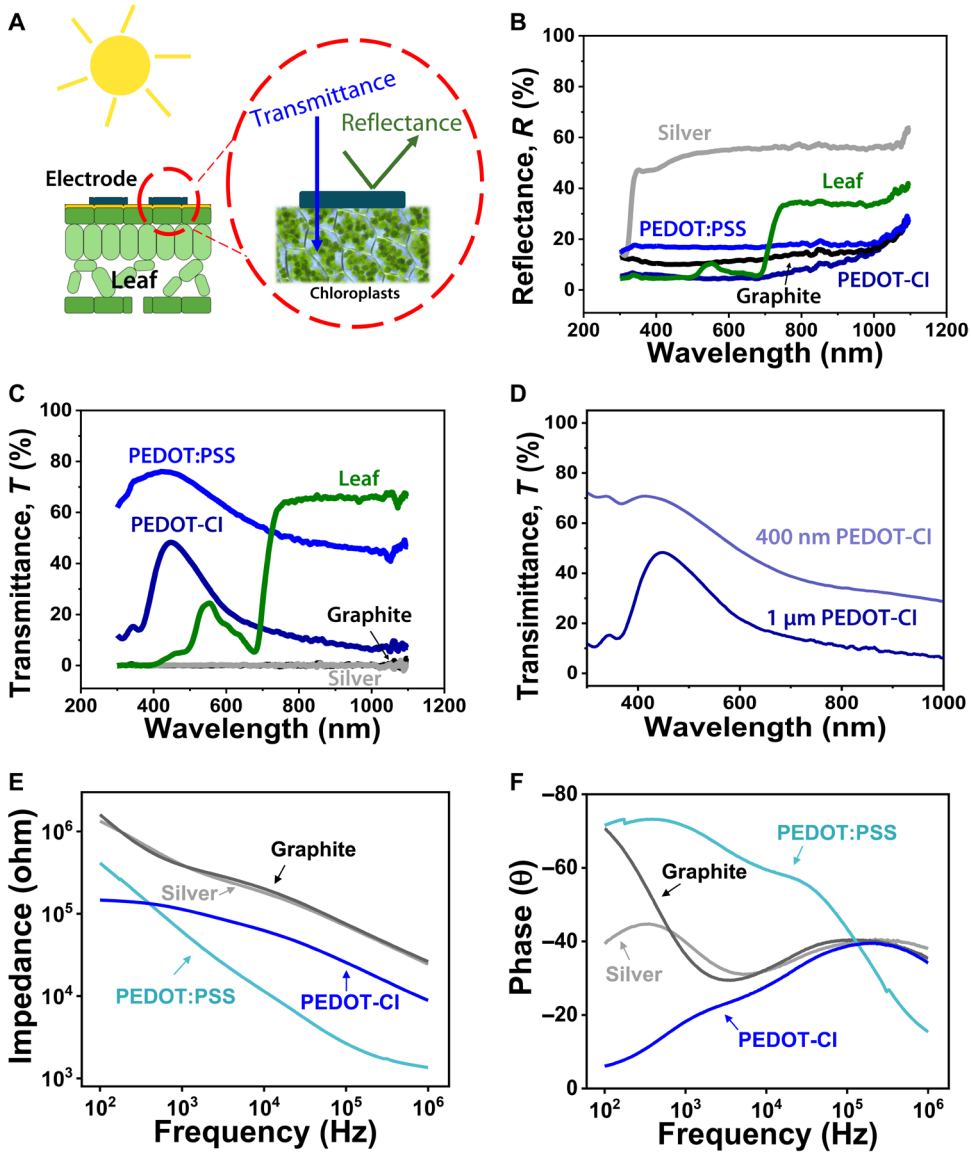

Fig. 2. Comparison of different electrode materials. (**A**) Cartoon depicting the influence of electrode transmittance and reflectance on the sunlight absorption ability of chloroplasts. (**B** and **C**) Reflectance and transmittance spectra of four different electrodes. All measurements were performed on glass substrates. The reflectance and transmittance spectra of a representative grape leaf are also provided. (**D**) Transmittance of a 400-nm-thick and a 1-µm-thick PEDOT-Cl film on glass. (**E** and **F**) Impedance and phase spectra obtained for a grape leaf using four different electrode materials.

Oxidative cell damage is thought to continue even after the source of ozone is removed. To probe this residual and continuing cellular damage, a few tattooed leaf samples were kept in water on a windowsill after exposure to 26.5 ppmh of ozone, and their impedance measured after 24 hours. While the leaves appeared nearly unchanged to the naked eye after 24 hours, as shown in Fig. 3, their impedance spectra revealed the presence of added cellular damage. The impedance decreased and the phase mismatch increased across the whole frequency range (Fig. 3, C and D) after 24 hours of aging after ozone treatment. This observation confirms that oxidative damage does not cease once the ozone source is removed and places emphasis on the need for early-stage interventions to prevent irreversible crop losses in commercial farms and orchards. We assume that these cumulative changes were induced by either dysfunction or death of cells caused by secondary chemical and/or biological damage resulting from severe ozone exposure (*44*).

As ozone is only generated when various nitrogen oxide (NO_x) species and volatile organic compounds (VOCs) in the atmosphere are decomposed by UV radiation (specifically UVA) from sunlight, we also considered NOx, VOCs, and UVA radiation as added stressors that could also potentially produce a change in the recorded impedance signal of tattooed leaves. Although VOCs have been implicated in a few observed effects on agriculture, a larger number of research studies performed across different growing zones have concluded that NO_x species are the primary cause of damage in food crops (*45*). In this case, plants are capable of selectively absorbing NO_x and chemically transforming these compounds into nutrients via a series of biological metabolisms (*46*). Thus, we tentatively ruled out

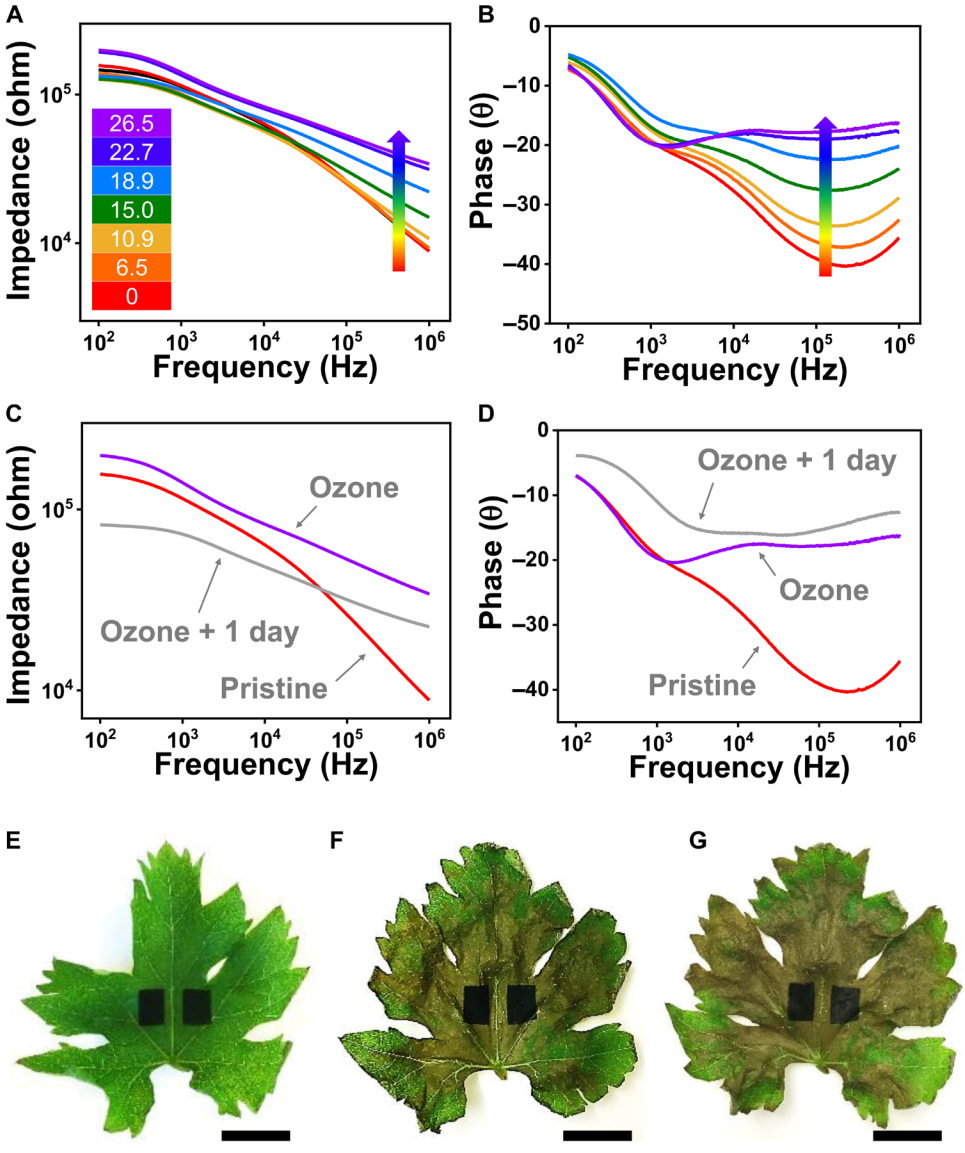

Fig. 3. Impedance measurements on ozone-treated grape leaves. (**A** and **B**) Impedance and phase of ozone-treated samples as a function of frequency. (**C** and **D**) Impedance and phase as a function of frequency for grape leaves aged in water for 1 day after ozone exposure. Images of (**E**) a pristine grape leaf, (**F**) the same leaf after 26.5 ppmh ozone exposure, and (**G**) the same leaf after being preserved in water for 1 day after ozone exposure. Scale bars, 10 mm. Photo credit: Jae Joon Kim, University of Massachusetts Amherst.

the possibility that NO_x would induce the same oxidative cell membrane collapse as ozone. On the other hand, in our previous paper (*47*), we investigated the effect of UVA radiation on the impedance signal of plant leaves. Upon UVA irradiation, the impedance signal in the 10^2- to 10^4-Hz region linearly decreased, and the peak frequency of the phase signal was shifted—these trends are the opposite of those recorded with ozone damage. Therefore, the distinctly different changes in impedance and phase produced by ozone and UVA damage are apparent enough to easily distinguish between these two stressors.

Drought stress can also cause crinkling and browning of leaf tissue, and these effects are hard to visually distinguish from necrotization due to oxidative damage (Fig. 4). To further confirm that the impedance changes discussed thus far were exclusively induced by ozone damage, drought conditions were also investigated. To simulate drought stress, we dried a fresh-picked, PEDOT-Cl tattooed grape leaf in a 50°C oven and measured its impedance signal every hour. The fresh-cut grape leaf had a relative water content of 80%, which decreased to 65% after drying for 24 hours. As shown in Fig. 4, the impedance globally increased with drying, likely arising from a decrease in overall ionic conductivity due to water loss, while the phase signal remained largely unchanged after being oven dried for 24 hours. After oven drying for 2 days, both impedance and phase plots exhibited intense and disordered changes, and the signals became much noisier after 4 days in an oven. These late-stage changes can be attributed to the deformation of the plant epidermis caused by dehydration of the leaf (*48*) and reduced ion mobility due to low water content. The phase versus frequency plots for oven-dried samples, even after 6 hours, looked reliably different from those of ozone-treated samples. Whereas ozone exposure caused a linear and sharp decrease in the phase at 10^5 Hz with increasing dose, this same signal

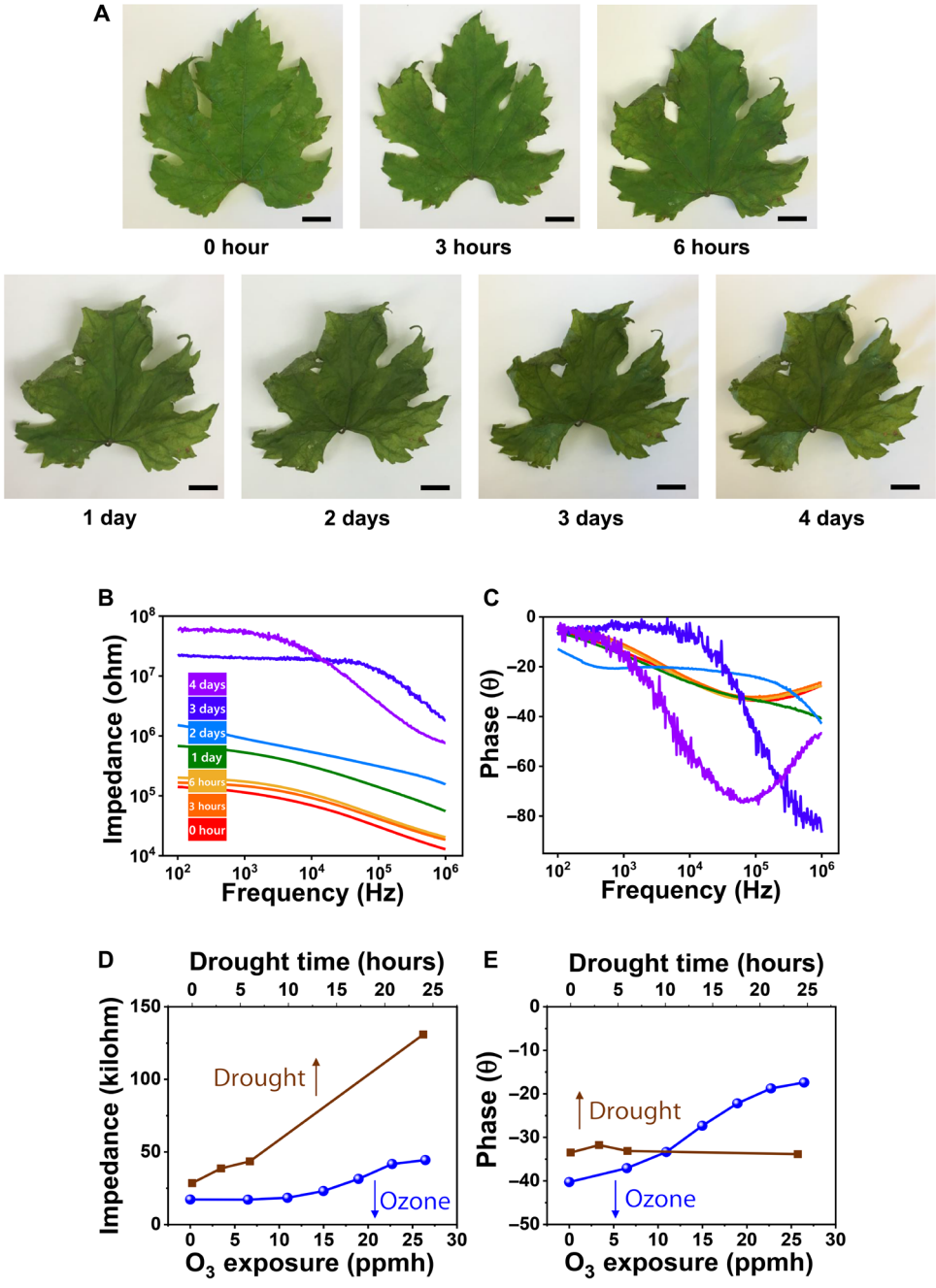

Fig. 4. Differentiation of impedance signals from different stressors. (**A**) Images of a grape leaf before and after drying in a 50°C oven to simulate drought stress. Scale bars, 10 mm. Photo credit: Jae Joon Kim, University of Massachusetts Amherst. (**B** and **C**) Impedance and phase of oven-dried samples as a function of frequency. (**D** and **E**) Comparison of the change in the impedance and phase signal at a frequency of 10^5 Hz between an oven-dried and an ozone-treated grape leaf.

remained constant in the oven-dried samples, thereby providing an easy approach to distinguish irreversible oxidative damage from reversible drought stress.

A leaf cell equivalent circuit model (fig. S8) was used to assign ozone-induced impedance and phase changes to particular cell components and to predict further changes upon aging. The model fitted the experimental impedance spectra well (fig. S9), thus intra- and extracellular resistances and membrane capacitances were extracted from the circuit simulations (table S1). The shift in impedance and phase could be specifically interpreted as a decrease in both membrane capacitance and ionic conductivity due to cell wall destruction and oxidation of intra- and extracellular fluids, respectively. These results were also consistent with previous reports (*33*). With added aging after exposure to ozone, the population of intact cells continues to diminish, thus further decreasing the membrane capacitance. Meanwhile, secondary oxidation of released fluid and/or membrane components creates mobile ions that increase the overall ionic conductivity of the sample, leading to globally higher impedance and phase values.

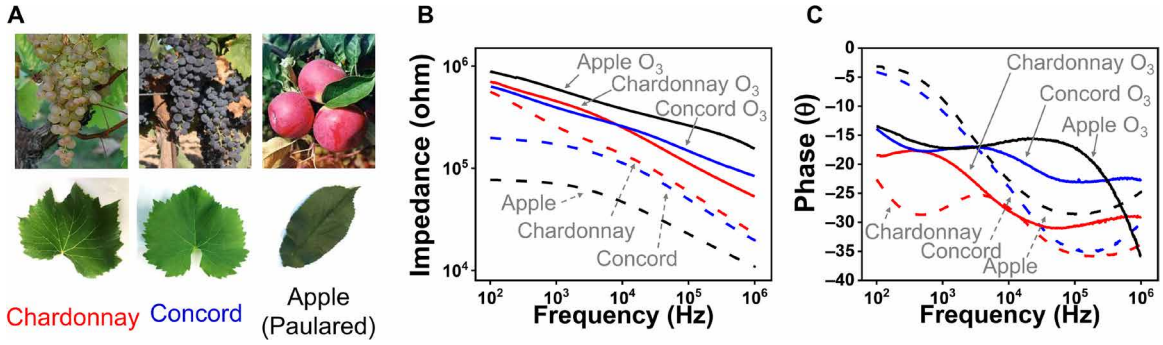

Fig. 5. Impedimetric detection of ozone damage in fruiting plants. (**A**) Images of different kinds of grape and apple leaves. Photo credit: Jae Joon Kim, University of Massachusetts Amherst. (**B** and **C**) Impedance and phase of each plant as a function of frequency before and after ozone exposure.

Last, we applied our detection method to observe ozone damage in different kinds of fruiting plants (Fig. 5): two different grape varieties and one common apple variety. The leaves of all investigated fruiting plants showed similar changes in impedance and phase signals at 10^5 Hz with ozone exposure as previously described, supporting the broad applicability of our method.

DISCUSSION

In this study, we propose the on-site electrical monitoring of ozone damage using vapor-deposited polymer tattoos and impedance spectroscopy. The oxidative damage caused when ozone and its by-products (collectively termed reactive oxygen species) interact with cellular components manifests as a unique change in the impedance and phase signal of leaf tissue, particularly at high frequencies. We use oCVD to create PEDOT-Cl films on the leaves of selected fruiting plants. These semipermanent PEDOT-Cl "tattoos" are uniquely ozone tolerant and capable of transducing biological ozone damage into a clear impedance change. Because each leaf tattoo retains the original electrode shape, size, and interelectrode spacing, impedance measurements can be performed on demand, at any time, with the assurance that variances in a signal over multiple measurements arise primarily due to changing plant health. Using an artificial ozone generator, we show that oxidative cell damage produces a clear, characteristic change in the high-frequency (10^4 to 10^6 Hz) impedance and phase signals of grape and apple leaves, which is not replicated by other common abiotic stressors, such as drought.

We expect that the detection of accumulated oxidative damage enabled by our method can contribute to the proper diagnosis of ozone damage. Specifically, if young seedlings and/or cuttings are tattooed and then planted at various strategic locations within a vineyard or orchard, these seedlings and cuttings can act as living sensors for ground-level ozone, potentially over many growing seasons, depending on whether the location experiences a hard frost in the winter. Periodic impedance signals recorded from the tattooed living sensors can result in the fast-tracking of on-time interventions to reduce ozone damage and increase crop yield.

MATERIALS AND METHODS

Materials and plants

All plant specimens were collected from Cold Spring Orchard Research and Education Center at the University of Massachusetts Amherst. Plants used in this study were Merlot, Chardonnay, and Concord grapes and Paulared apple leaves. 3,4-Ethylenedioxythiophene (EDOT), iron chloride ($FeCl_3$), and PEDOT:PSS (1 weight % in water) were purchased from Sigma-Aldrich. PELCO colloidal graphite paste and PELCO conductive silver paste were purchased from Ted Pella. All chemicals were used without any purification. A commercial hydrogel (Water Storing Crystals, Miracle-Gro Lawn Products Inc.) was used to maintain a constant hydration level in cut samples during the vapor deposition.

Electrodes

Fresh leaves were picked from 3-year-old plants, rinsed with distilled water, and air dried for 10 min. To maintain freshness, the cut leaves were placed in water immediately before and immediately after the deposition process. To create spatially patterned electrodes, a plastic shadow mask was prepared by cutting the desired pattern into a polyethylene terephthalate (PET) sheet, the mask placed directly on the leaf surface, and its edges affixed to the leaf surface using painter's tape, which yielded sharp pattern edges and did not damage the leaves in the process. The mask and tape were lifted off immediately after the deposition.

To prevent dehydration during the deposition, the cut edge of the stem of the leaf was placed in contact with a water-swelled hydrogel, wrapped tightly with plastic wrap, and then sealed with paraffin wax to create a vacuum-insensitive hydration pocket that ensured continuous hydration. Samples were then affixed to the sample stage inside our custom-built vapor deposition chamber without any surface treatments.

EDOT (monomer) was directly polymerized on the surface of leaves via oCVD as reported previously (*26*). In the current study, the entire deposition time lasted approximately 40 min, including preheating of oxidant and monomer, oCVD, and cooling/venting processes, during which the deposition pressure was maintained at 1 ± 0.1 torr, depending on sample conditions. The solid oxidant $FeCl_3$ was placed inside a ceramic crucible and heated by electrical furnace, while monomer was stored in an ampule and heated to 110°C. When oxidant sublimed at around 200°C, monomer inlet was introduced into the chamber by adjusting a needle valve to maintain the monomer-to-oxidant ratio. To further minimize dehydration during the deposition, the temperature of the sample stage was maintained at 25°C with a temperature controller. Polymer coating thickness and evaporation rates of EDOT and $FeCl_3$ were monitored in real time by a quartz crystal microbalance (QCM)

sensor situated near the sample stage with the maximum rate 2 nm/s and the until polymer thickness reached 1 μm. After deposition, the residual oxidant and monomer were removed from the PEDOT-Cl–coated samples by dipping the leaves into a dilute acid solution (0.1 mM) for 1 min and, subsequently, distilled water for 5 min.

Optical and electrical characterization

The optical images and videos of samples were captured with an optical microscope (Mighty Scope, Aven) and a digital camera (K-30, Pentax). Scanning electron micrographs (SEMs) were captured using Magellan 400 XHR SEM. The surface conductivities of PEDOT, silver paint, and graphite on plant leaves were measured using a four-probe measurement station (Pro4-440 N, Lucas Labs) equipped with an SP4 probe head. The tip spacing was 0.050 inch, and tip radius was 0.0016 inch. The tip was made of tungsten carbide.

For the bending and adhesion tests, leaves coated with different electrodes were wrapped around three-dimensional–printed cylinders of varying diameters (3 to 10 mm) to simulate strain. Alligator clips were used to make stable electrical contacts to the polymer coating while bending. Rinsing test was performed by putting the sample under continuously flowing water (5 liter/min) with the tap diameter of 10 mm for 10 min. For testing the electrode stability in the aqueous and saline (1 M, approximately similar to seawater concentration), the electrodes on leaves were immersed in those solutions for 1 day, and their conductivities were measured after the surface was air dried. A UV-vis spectrophotometer (Evolution 220, Thermo Fisher Scientific) was used to study the transmittivity and reflectance of the electrodes on leaf surfaces.

Ozone treatment

Ozone treatment was established using an ozone generator (7000-OG, Star Knight Inc.), and the generation rate was measured with a gas sampling pump (BH-GSP, BOSEAN) and a O_3 gas detector (BH-90A, BOSEAN). Ozone gas was generated in a sealed box with one outlet for gas sampling at the bottom. As shown in fig. S7, the measured ozone doses over each 30-min interval were 6.5, 10.9, 15.0, 18.9, 22.7, and 26.5 ppmh, respectively. Polymer electrodes were vapor deposited onto leaves before ozone treatment. Samples were placed facedown right next to the outlet of the ozone generator to expose the abaxial side (bottom face) of the leaf where stomata are positioned. To prevent sample dehydration during irradiation, the cut ends of the leaves were packed with a water-soaked cotton ball. Impedance for Merlot leaves was measured every half hour.

Aging and drought

Aging treatment was performed by analyzing an ozone-exposed grape leaf (26.5 ppmh of ozone exposure) after being stored in water for 1 day (approximately 10 hours of sunlight exposure). For the drought test, a cut leaf was placed in a 50°C oven without being placed into water.

Impedance measurements

Impedance measurements were performed using an Agilent 4292A precision impedance analyzer over the frequency range of 10^2 to 10^6 Hz and a low applied potential of 500 mV to prevent any undesirable chemical reactions. Two PEDOT-Cl electrodes of 5-mm width and 10-mm length were placed 10 mm away and covered with a droplet of 0.1 M saline. Metal probe tips mounted on a micromanipulator then were lowered into the droplets to make electrical contact between instrument and custom-built station. Saline droplets were rinsed away with distilled water after each measurement. PEDOT:PSS, silver, and graphite ink were treated in the same way.

Equivalent circuit models for impedance spectroscopy

Zview2 software (Princeton Applied Research) was used to iteratively fit experiment data to an equivalent circuit and extract values of each circuit component.

SUPPLEMENTARY MATERIALS

Supplementary material for this article is available at http://advances.sciencemag.org/cgi/content/full/6/36/eabc3296/DC1

View/request a protocol for this paper from *Bio-protocol*.

REFERENCES AND NOTES

1. H. Pleijel, M. C. Broberg, J. Uddling, G. Mills, Current surface ozone concentrations significantly decrease wheat growth, yield and quality. *Sci. Total Environ.* **613-614**, 687–692 (2018).
2. E. A. Ainsworth, Understanding and improving global crop response to ozone pollution. *Plant J.* **90**, 886–897 (2017).
3. S. Avnery, D. L. Mauzerall, J. Liu, L. W. Horowitz, Global crop yield reductions due to surface ozone exposure: 2. Year 2030 potential crop production losses and economic damage under two scenarios of O_3 pollution. *Atmos. Environ.* **45**, 2297–2309 (2011).
4. E. A. Ainsworth, Rice production in a changing climate: A meta-analysis of responses to elevated carbon dioxide and elevated ozone concentration. *Glob. Chang. Biol.* **14**, 1642–1650 (2008).
5. E. A. Ainsworth, S. P. Serbin, J. A. Skoneczka, P. A. Townsend, Using leaf optical properties to detect ozone effects on foliar biochemistry. *Photosynth. Res.* **119**, 65–76 (2014).
6. A. Y. Khaled, S. A. Aziz, S. K. Bejo, N. M. Nawi, I. A. Seman, D. I. Onwude, Early detection of diseases in plant tissue using spectroscopy–applications and limitations. *Appl. Spectrosc. Rev.* **53**, 36–64 (2018).
7. F. Faoro, M. Iriti, Cell death behind invisible symptoms: Early diagnosis of ozone injury. *Biol. Plant.* **49**, 585–592 (2005).
8. W. Van Camp, H. Willekens, C. Bowler, M. Van Montagu, D. Inzé, P. Reupold-Popp, H. Sandermann Jr., C. Langebartels, Elevated levels of superoxide dismutase protect transgenic plants against ozone damage. *Biotechnol.* **12**, 165–168 (1994).
9. B. B. Moura, E. S. Alves, M. A. Marabesi, S. R. Souza, M. Schaub, P. Vollenweider, Ozone affects leaf physiology and causes injury to foliage of native tree species from the tropical atlantic forest of southern brazil. *Sci. Total Environ.* **610-611**, 912–925 (2018).
10. W. J. Massman, R. C. Musselman, A. S. Lefohn, A conceptual ozone dose-response model to develop a standard to protect vegetation. *Atmos. Environ.* **34**, 745–759 (2000).
11. L. D. Emberson, M. R. Ashmore, H. M. Cambridge, D. Simpson, J.-P. Tuovinen, Modelling stomatal ozone flux across europe. *Environ. Pollut.* **109**, 403–413 (2000).
12. E. Paoletti, A. Alivernini, A. Anav, O. Badea, E. Carrari, S. Chivulescu, A. Conte, M. L. Ciriani, L. Dalstein-Richier, A. De Marco, S. Fares, G. Fasano, A. Giovannelli, M. Lazzara, S. Leca, A. Materassi, V. Moretti, D. Pitar, I. Popa, F. Sabatini, L. Salvati, P. Sicard, T. Sorgi, Y. Hoshika, Toward stomatal–flux based forest protection against ozone: The MOTTLES approach. *Sci. Total Environ.* **691**, 516–527 (2019).
13. M. Jezek, A. Hills, M. R. Blatt, V. L. Lew, A constraint–relaxation–recovery mechanism for stomatal dynamics. *Plant Cell Environ.* **42**, 2399–2410 (2019).
14. S. Fares, A. Conte, A. Chabbi, Ozone flux in plant ecosystems: New opportunities for long-term monitoring networks to deliver ozone-risk assessments. *Environ. Sci. Pollut. Res.* **25**, 8240–8248 (2018).
15. M. H. Wong, J. P. Giraldo, S.-Y. Kwak, V. B. Koman, R. Sinclair, T. T. S. Lew, G. Bisker, P. Liu, M. S. Strano, Nitroaromatic detection and infrared communication from wild-type plants using plant nanobionics. *Nat. Mater.* **16**, 264–272 (2017).
16. S. Zhuang, L. Zhou, W. Xu, N. Xu, X. Hu, X. Li, G. Lv, Q. Zheng, S. Zhu, Z. Wang, J. Zhu, Tuning transpiration by interfacial solar absorber-leaf engineering. *Adv. Sci.* **5**, 1700497 (2018).
17. J. P. Giraldo, M. P. Landry, S. M. Faltermeier, T. P. McNicholas, N. M. Iverson, A. A. Boghossian, N. F. Reuel, A. J. Hilmer, F. Sen, J. A. Brew, M. S. Strano, Plant nanobionics approach to augment photosynthesis and biochemical sensing. *Nat. Mater.* **13**, 400 (2014).
18. S.-Y. Kwak, J. P. Giraldo, M. H. Wong, V. B. Koman, T. T. S. Lew, J. Ell, M. C. Weidman, R. M. Sinclair, M. P. Landry, W. A. Tisdale, M. S. Strano, A nanobionic light-emitting plant. *Nano Lett.* **17**, 7951–7961 (2017).
19. Y. Jie, X. Jia, J. Zou, Y. Chen, N. Wang, Z. L. Wang, X. Cao, Natural leaf made triboelectric nanogenerator for harvesting environmental mechanical energy. *Adv. Energy Materi.* **8**, 1703133 (2018).

20. Y. Chen, Y. Jie, J. Wang, J. Ma, X. Jia, W. Dou, X. Cao, Triboelectrification on natural rose petal for harvesting environmental mechanical energy. *Nano Energy* **50**, 441–447 (2018).
21. E. Stavrinidou, R. Gabrielsson, E. Gomez, X. Crispin, O. Nilsson, D. T. Simon, M. Berggren, Electronic plants. *Sci. Adv.* **1**, e1501136 (2015).
22. E. Stavrinidou, R. Gabrielsson, K. P. R. Nilsson, S. K. Singh, J. F. Franco-Gonzalez, A. V. Volkov, M. P. Jonsson, A. Grimoldi, M. Elgland, I. V. Zozoulenko, D. T. Simon, M. Berggren, In vivo polymerization and manufacturing of wires and supercapacitors in plants. *Proc. Natl. Acad. Sci. U.S.A.* **114**, 2807–2812 (2017).
23. D. J. Poxson, M. Karady, R. Gabrielsson, A. Y. Alkattan, A. Gustavsson, S. M. Doyle, S. Robert, K. Ljung, M. Grebe, D. T. Simon, M. Berggren, Regulating plant physiology with organic electronics. *Proc. Natl. Acad. Sci. U.S.A.* **114**, 4597–4602 (2017).
24. I. Bernacka-Wojcik, M. Huerta, K. Tybrandt, M. Karady, M. Y. Mulla, D. J. Poxson, E. O. Gabrielsson, K. Ljung, D. T. Simon, M. Berggren, E. Stavrinidou, Implantable organic electronic ion pump enables ABA hormone delivery for control of stomata in an intact tobacco plant. *Small* **15**, e1902189 (2019).
25. N. Coppedè, M. Janni, M. Bettelli, C. L. Maida, F. Gentile, M. Villani, R. Ruotolo, S. Iannotta, N. Marmiroli, M. Marmiroli, A. Zappettini, An *in vivo* biosensing, biomimetic electrochemical transistor with applications in plant science and precision farming. *Sci. Rep.* **7**, 16195 (2017).
26. J. J. Kim, L. K. Allison, T. L. Andrew, Vapor-printed polymer electrodes for long-term, on-demand health monitoring. *Sci. Adv.* **5**, eaaw0463 (2019).
27. V. B. Koman, T. T. S. Lew, M. H. Wong, S.-Y. Kwak, J. P. Giraldo, M. S. Strano, Persistent drought monitoring using a microfluidic-printed electro-mechanical sensor of stomata *in planta*. *Lab Chip* **17**, 4015–4024 (2017).
28. K. Lee, J. Park, M.-S. Lee, J. Kim, B. G. Hyun, D. J. Kang, K. Na, C. Y. Lee, F. Bien, J.-U. Park, In-situ synthesis of carbon nanotube–graphite electronic devices and their integrations onto surfaces of live plants and insects. *Nano Lett.* **14**, 2647–2654 (2014).
29. J. M. Nassar, S. M. Khan, D. R. Villalva, M. M. Nour, A. S. Almuslem, M. M. Hussain, Compliant plant wearables for localized microclimate and plant growth monitoring. *npj Flex. Electron.* **2**, 24 (2018).
30. G. Soja, M. Eid, H. Gangl, H. Redl, Ozone sensitivity of grapevine (*Vitis vinifera* L.): Evidence for a memory effect in a perennial crop plant? *Phyton* **37**, 265–270 (1997).
31. G. Soja, T. G. Reichenauer, M. Eid, A.-M. Soja, R. Schaber, H. Gangl, Long-term ozone exposure and ozone uptake of grapevines in open-top chambers. *Atmos. Environ.* **38**, 2313–2321 (2004).
32. A. Valletta, E. Salvatori, A. R. Santamaria, M. Nicoletti, C. Toniolo, E. Caboni, A. Bernardini, G. Pasqua, F. Manes, Ecophysiological and phytochemical response to ozone of wine grape cultivars of *Vitis vinifera* L. *Nat. Prod. Res.* **30**, 2514–2522 (2016).
33. T. Repo, E. Oksanen, E. Vapaavuori, Effects of elevated concentrations of ozone and carbon dioxide on the electrical impedance of leaves of silver birch (*Betula pendula*) clones. *Tree Physiol.* **24**, 833–843 (2004).
34. A. Martin, B. S. Chang, Z. Martin, D. Paramanik, C. Frankiewicz, S. Kundu, I. D. Tevis, M. Thuo, Heat-free fabrication of metallic interconnects for flexible/wearable devices. *Adv. Funct. Mater.* **29**, 1903687 (2019).
35. L. R. Thorne, Oxidation of Thin Silver Films by Ozone and Atomic Oxygen, in *Undergraduate Honors Capstone Projects* (1973), vol. 177.
36. J. M. Simmons, B. M. Nichols, S. E. Baker, M. S. Marcus, O. M. Castellini, C.-S. Lee, R. J. Hamers, M. A. Eriksson, Effect of ozone oxidation on single-walled carbon nanotubes. *J. Phys. Chem. B* **110**, 7113–7118 (2006).
37. T. Nagata, S. Oh, T. Chikyow, Y. Wakayama, Effect of UV-ozone treatment on electrical properties of PEDOT:PSS film. *Org. Electron.* **12**, 279–284 (2011).
38. X. Wang, X. Zhang, L. Sun, D. Lee, S. Lee, M. Wang, J. Zhao, Y. Shao-Horn, M. Dincă, T. Palacios, K. K. Gleason, High electrical conductivity and carrier mobility in oCVD PEDOT thin films by engineered crystallization and acid treatment. *Sci. Adv.* **4**, eaat5780 (2018).
39. M. Heydari Gharahcheshmeh, K. K. Gleason, Device fabrication based on oxidative chemical vapor deposition (oCVD) synthesis of conducting polymers and related conjugated organic materials. *Adv. Mater. Interfaces* **6**, 1801564 (2019).
40. O. G. Martinsen, S. Grimnes, *Bioimpedance and Bioelectricity Basics* (Academic press, 2011).
41. M. Grossi, B. Riccò, Electrical impedance spectroscopy (EIS) for biological analysis and food characterization: A review. *J. Sens. Sensor Syst.* **6**, 303–325 (2016).
42. A. Angersbach, V. Heinz, D. Knorr, Evaluation of process-induced dimensional changes in the membrane structure of biological cells using impedance measurement. *Biotechnol. Prog.* **18**, 597–603 (2002).
43. D. Tomkiewicz, T. Piskier, A plant based sensing method for nutrition stress monitoring. *Precis. Agric.* **13**, 370–383 (2012).
44. W. L. Chameides, The chemistry of ozone deposition to plant leaves: Role of ascorbic acid. *Environ. Sci. Technol.* **23**, 595–600 (1989).
45. X. Wei, J. Chen, Y. Yu, Z. Wang, H. Liu, D. Pan, J. Chen, Phylloremediation of air pollutants: Exploiting the potential of plant leaves and leaf-associated microbes. *Front. Plant Sci.* **8**, 1318 (2017).
46. J. N. Cape, Effects of airborne volatile organic compounds on plants. *Environ. Pollut.* **122**, 145–157 (2003).
47. J. J. Kim, T. L. Andrew, Real-time and noninvasive detection of UV-induced deep tissue damage using electrical tattoos. *Biosens. Bioelectron.* **150**, 111909 (2020).
48. Y. Ando, K. Mizutani, N. Wakatsuki, Electrical impedance analysis of potato tissues during drying. *J. Food Eng.* **121**, 24–31 (2014).
49. M. I. N. Zhang, J. H. M. Willison, Electrical impedance analysis in plant tissues11. *J. Exp. Bot.* **42**, 1465–1475 (1991).
50. C. H. Hsu, F. Mansfeld, Concerning the conversion of the constant phase element parameter Y_0 into a capacitance. *Corrosion* **57**, 747–748 (2001).

Acknowledgments: We thank M. Formosi from the Durfee Conservatory and L. Ware and E. Petit at the University of Massachusetts Amherst for providing a wide variety of plant leaf samples. We also thank H. Yuk for valuable discussions. **Funding:** This material is based on work supported by the National Science Foundation under CHEM MSN 1807743. J.J.K. gratefully acknowledges support from the Nuclear Global Postdoc Fellowship Program provided by the Korea Nuclear International Cooperation Foundation (KONICOF). **Author contributions:** J.J.K. and T.L.A. conceptualized the study and designed the experiments. T.L.A. raised funds to support this study. J.J.K., R.F., and L.K.A. prepared the leaf samples. J.J.K. and R.F. performed impedance measurements and analyzed the data. J.J.K., R.F., and T.L.A. wrote the paper. **Competing interests:** The authors declare that they have no competing interests. **Data and materials availability:** All data needed to evaluate the conclusions in the paper are present in the paper and/or the Supplementary Materials. Additional data related to this paper may be requested from the authors.

Submitted 18 April 2020
Accepted 13 July 2020
Published 4 September 2020
10.1126/sciadv.abc3296

Citation: J. J. Kim, R. Fan, L. K. Allison, T. L. Andrew, On-site identification of ozone damage in fruiting plants using vapor-deposited conducting polymer tattoos. *Sci. Adv.* **6**, eabc3296 (2020).

Science Advances

On-site identification of ozone damage in fruiting plants using vapor-deposited conducting polymer tattoos

Jae Joon Kim, Ruolan Fan, Linden K. Allison and Trisha L. Andrew

Sci Adv **6** (36), eabc3296.
DOI: 10.1126/sciadv.abc3296

Science Advances (ISSN 2375-2548) is published by the American Association for the Advancement of Science, 1200 New York Avenue NW, Washington, DC 20005. The title *Science Advances* is a registered trademark of AAAS.